# Fluorescent Hydroxyl Emissions from Saturn's Ring Atmosphere

Doyle T. Hall, Paul D. Feldman, J. B. Holberg, Melissa A. McGrath

Just before Earth passed through Saturn's ring plane on 10 August 1995, the Hubble Space Telescope Faint Object Spectrograph detected ultraviolet fluorescent emissions from a tenuous atmosphere of OH molecules enveloping the rings. Brightnesses decrease with increasing distance above the rings, implying a scale height of about 0.45 Saturn radii ($R_S$). A spatial scan $0.28R_S$ above the A and B rings indicates OH column densities of about $10^{13}$ cm$^{-2}$ and number densities of up to 700 cm$^{-3}$. Saturn's rings must produce roughly $10^{25}$ to $10^{29}$ OH molecules per second to maintain the observed OH distribution.

The discovery of the icy composition of Saturn's rings (*1*) led to the prediction of a tenuous atmosphere of water vapor and other gaseous water dissociation products (including OH, O, and H) enveloping the ring system (*2*), much like the coma that enshrouds the icy nucleus of a comet. With the advent of rocket-borne and spacecraft ultraviolet instruments, this prediction was confirmed by the detection of hydrogen Lyman-$\alpha$ radiation from the vicinity of the rings, indicating an H atom density of 400 to 600 cm$^{-3}$ (*3, 4*). Subsequent charged-particle measurements from the Pioneer and Voyager spacecraft indicated that Saturn's inner magnetosphere is populated with water-group ions partially derived from ionization of the neutral gas in the ring atmosphere (*5, 6*). These spacecraft also revealed a substantial influx of water into Saturn's ionosphere from the rings (*7*).

Early suggestions for the sources of the ring atmosphere included sublimation, charged-particle sputtering, and photosputtering of Saturn's icy ring particles and inner satellites, but these processes failed to explain quantitatively the observed H density near the rings (*5*). In addition, the question of hydrogen gas source rates is complicated by the existence of a larger H cloud extending from outside Titan's orbit inward nearly to Saturn (*4, 8*). This cloud derives its material from several sources, including the upper atmospheres of Titan and Saturn (*8*), and makes it difficult to determine the H gas production rate from the rings alone. However, detailed models have demonstrated that meteoritic bombardment and vaporization of the ring particles and inner satellites should produce significant quantities of gas (*9*), including water vapor and other oxygen-bearing species (*10–12*). Because these oxygen-bearing gases are unlikely to originate from Saturn's atmosphere, measuring their density and distribution provides a less ambiguous measure of the erosion rate of the icy ring particles by meteoritic impacts and other processes. This is an important consideration because, although outer solar system meteoritic impact rates are extremely uncertain, impact erosion can in principle limit the lifetime of Saturn's rings to much less than the known age of the solar system (*9, 10, 13*).

Shemansky *et al.* (*14*) first used the Hubble Space Telescope (HST) to detect OH $A^2\Sigma^+$-$X^2\Pi$ (0,0) band emissions (*15*) from the Saturn system at an equatorial distance of 4.5 Saturn radii ($1R_S$ = 60,330 km), a location between the orbits of the satellites Enceladus and Dione, well outside the main ring system. Possible sources for this extended OH gas cloud include micrometeorite impact (*14*), charged-particle sputtering (*16*), and collisions of E-ring grains with the icy satellites (*17*). Here we extend the study of the Saturn-system OH distribution using HST observations scheduled to coincide with a Saturn ring-plane crossing event, providing a rare opportunity to measure OH fluorescence directly above the ring plane.

During six HST orbits that preceded the 10 August 1995 ring-plane crossing event by less than 36 hours, the Faint Object Spectrograph (FOS) acquired spectra at five locations above Saturn's ring plane (Table 1). The FOS RED detector and G270H grating provided wavelength coverage from 2220 to 3280 Å, with an effective spectral resolution of about 24 Å for diffuse sources filling the aperture, well suited to measure the OH $A^2\Sigma^+$-$X^2\Pi$ (0,0) band, which has emission lines extending from 3070 to 3110 Å (*15*). The largest available spectrograph aperture (3.66 arc sec by 1.29 arc sec) was used for maximum throughput. The five target locations were selected to provide scans of the emission both perpendicular to the ring plane (1, 2, and 3) and parallel to the ring plane (1, 4, and 5). Target positions 1, 4, and 5 were selected to measure the emission as close to the ring plane as possible and to prevent the rings or any of Saturn's satellites from entering the aperture; the relatively intense reflected sunlight from these objects would have contaminated the spectra, severely reducing the chance of detecting the faint fluorescent emission from the ring atmosphere.

An important consideration in observations of Saturn-system OH fluorescence is light from nearby bright objects (not within the spectrograph entrance aperture) that is scattered inside the HST optical assembly into the FOS instrument (*14, 18*). When Saturn's rings are not viewed edge-on, scattered light from the rings produces a large contaminating signal precluding measurements in the vicinity of the rings. The HST Wide Field Planetary Camera 2 (WFPC-2) images acquired during the 1995 ring-plane crossing events reveal that the largest source of scattered light is Saturn, although the inner satellites and edge-on rings contribute as well (*19*). Because the spectra of these objects in the 2990 to 3200 Å wavelength range are dominated by reflected sunlight, the scattered light was modeled by convolving a reflected solar spectrum with the FOS line-spread function for a diffuse source that fills the aperture (*14, 18*). Modeled scattered-light spectra were scaled to fit the observed spectra in two wavelength ranges that bracket the OH emission and were then subtracted from the observed

**Table 1.** Saturn ring atmosphere OH $A^2\Sigma^+$-$X^2\Pi$ (0,0) band observations. The dates are universal times (UT) spanned by the observations. The position of the center of the FOS aperture is measured by $x$ (parallel to ring plane) and $z$ (perpendicular) relative to the center of Saturn. The brightness is based on the integrated flux in the 3060 to 3110 Å range. The quoted uncertainties are the estimated 1$\sigma$ errors due to both statistical uncertainties and scattered-light subtraction.

| Target | Date | Duration (s) | $x$ ($R_S$) | $z$ ($R_S$) | $B$ (R) |
|---|---|---|---|---|---|
| 1 | 9 Aug 1995, 11:52–13:59 | 3605 | 1.9 | 0.28 | 79 ± 17 |
| 2 | 9 Aug 1995, 14:57–15:30 | 1663 | 1.9 | 0.40 | 62 ± 12 |
| 3 | 9 Aug 1995, 16:34–17:37 | 2035 | 1.9 | 0.60 | 20 ± 13 |
| 4 | 10 Aug 1995, 11:52–12:29 | 1895 | 2.1 | 0.28 | 87 ± 23 |
| 5 | 10 Aug 1995, 10:19–10:56 | 1915 | 2.3 | 0.28 | 111 ± 12 |

D. T. Hall and P. D. Feldman, Center for Astrophysical Sciences, Department of Physics and Astronomy, Johns Hopkins University, Baltimore, MD 21218, USA. E-mail: dthall@pha.jhu.edu
J. B. Holberg, Lunar and Planetary Laboratory, University of Arizona, Tucson, AZ 85716, USA. E-mail: holberg@argus.lpl.arizona.edu
M. A. McGrath, Space Telescope Science Institute, 3700 San Martin Drive, Baltimore, MD 21218, USA. E-mail: mcgrath@stsci.edu

spectra to produce residual spectra (*20*). Emissions from Saturn's ring atmosphere identified in the residual spectra agree with the expected spectral shape for the OH $A^2\Sigma^+$-$X^2\Pi$ (0,0) emissions (*21*) to within statistical measurement uncertainty (Fig. 1). The OH band brightnesses were derived by integration of the residual spectra between 3060 and 3110 Å (Table 1) and vary from about 20 to 110 rayleighs (R) (*22*).

Estimates of OH molecule abundance can be calculated from observed brightnesses with use of the $A^2\Sigma^+$-$X^2\Pi$ (0,0) band fluorescence efficiency, the *g* factor, which is a measure of the number of photons emitted per molecule per second. Because strong Fraunhofer lines in the near-ultraviolet solar spectrum excite many of the fluorescent band emissions, OH molecules with different heliocentric radial speeds are subject to different Doppler wavelength shifts and fluoresce at different rates (*15*). This effect complicates the analysis of the ring atmosphere observations, because the OH molecules will have a distribution of velocities at any point in the Saturn system, and along any sight line the *g* factor will vary significantly. Two different model calculations of a meteorite-generated ring atmosphere (*11, 12*) indicate that most of the oxygen-bearing neutral gas is confined to equatorial distances between $1.2R_S$ and $2.8R_S$. Assuming that the OH molecules are in circular orbits confined to this region, we have calculated that heliocentric radial speeds along the observational sight lines vary over the range 10 to 18 km $s^{-1}$. At the heliocentric distance of Saturn during the observations (9.62 astronomical units), this velocity range indicates that *g* factors vary from $5 \times 10^{-6}$ to $10 \times 10^{-6}$ $s^{-1}$, with an average value of $9 \times 10^{-6}$ $s^{-1}$ (*15*). A rigorous analysis will require a detailed estimate of the dispersion of OH molecule velocities along any sight line. We have neglected this complication and have performed an approximate analysis using a constant value of $g \approx 9 \times 10^{-6}$ $s^{-1}$.

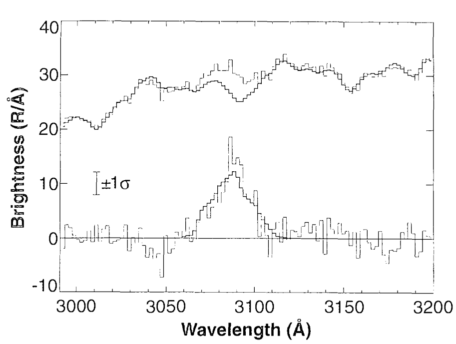


**Fig. 1.** The HST FOS spectrum acquired at target 5 above Saturn's rings. The upper histogram shows the observed brightness between wavelengths 2990 and 3200 Å (thin line), accumulated in bins with widths of one FOS detector diode, with the model scattered-light spectrum overplotted (thick line). The lower histogram shows the residual emissions (after subtraction of the scattered light) multiplied by 3 for clarity (thin line) and the expected shape of the OH $A^2\Sigma^+$-$X^2\Pi$ (0,0) fluorescent emission convolved with the FOS line-spread function with the same integrated brightness (thick line). The representative $\pm 1\sigma$ error bar shown on the left (also multiplied by 3) illustrates that the spectral shapes of the observed residual ring atmosphere emissions and the OH fluorescent emissions agree to within statistical measurement uncertainty.

In this approximation, OH column densities are given by $N = 10^6 B/g$, where *B* denotes the brightness in rayleighs. Aperture-averaged column densities $\bar{N}$ vary over the range $0.2 \times 10^{13}$ to $1.2 \times 10^{13}$ $cm^{-2}$ for the five targets. The measurements closest to the ring plane (targets 1, 4, and 5) suggest an increase in abundance with increasing equatorial distance, with $\bar{N}$ varying from $0.9 \times 10^{13}$ to $1.2 \times 10^{13}$ $cm^{-2}$. The scan perpendicular to the rings (targets 1, 2, and 3) indicates that OH column densities decrease monotonically with increasing distance *z* above the ring plane. If the column density is modeled by the formula $N = N_0 e^{-(z/H)^2}$, expected for a population of particles in a distribution of Keplerian orbits (*23*), the best-fit scale height is $H \approx 0.45R_S$, with a $2\sigma$ (95%) confidence interval of $0.36R_S$ to $0.66R_S$ (*24*).

Calculating average OH number densities requires estimates of the path length along any given sight line through the emission volume and thus requires a knowledge of the spatial distribution of OH in the Saturn system. If most of the gas is confined to equatorial distances between $1.2R_S$ and $2.8R_S$ (*11, 12*), then path lengths of $3R_S$ to $4R_S$ are appropriate. Such distances indicate OH densities in the range 350 to 500 $cm^{-3}$ for target 1 and 500 to 700 $cm^{-3}$ for target 5. These ranges are upper limits because we have neglected the contribution from the OH gas that is known to exist at larger equatorial distances from Saturn (*14*). It is unlikely that this more extended OH cloud accounts for all of the observed emissions because it is physically implausible that it could produce the ≈40% increase in brightness observed over the relatively short ($\approx 0.4R_S$) interval from target 1 to target 5. Assuming that all of this ≈40% increase is due to the ring atmosphere gas and that the remainder of the emission is from the more extended OH cloud yields a lower limit density of about 150 $cm^{-3}$ for target 5.

The pattern of increasing brightnesses with increasing equatorial distance suggests the existence of a toroidal OH distribution with maximum density occurring outside the main ring system and may be related to the process thought to limit most severely the lifetime of ring atmosphere neutrals: physical adhesion to icy ring particles during collisions (*11, 12, 25*). Molecules in Keplerian orbits with finite inclination generally cross the ring plane twice per orbit. If the crossings occur in the densest rings (A and B), which have normal optical depths of about one, then the probability of the molecule encountering and sticking to a ring particle is much greater than if the crossings occur outside the main ring system, where optical depths are two to three orders of magnitude smaller (*11, 23*). Thus, the dynamical lifetime of OH molecules in orbits of moderate eccentricity probably increases dramatically just beyond the outermost extension of the A ring ($2.27R_S$), which might explain the increasing brightnesses. However, in light of the facts that the observational sight lines traverse the entire Saturn system and that *g* factors depend sensitively on heliocentric radial speed, this theory may not be a unique interpretation.

To obtain an estimate of how quickly the ring system produces OH gas, we assume that the ring atmosphere is confined between equatorial radii $1.2R_S$ and $2.8R_S$ (*11, 12*) and that the OH density in this region is given by $n = n_0 e^{-(z/H)^2}$, where $H \approx 0.45R_S$. To reproduce observed brightnesses for targets 1, 4, and 5 from such a distribution (*24*) requires $n_0 \approx 500$ to 900 $cm^{-3}$. If all of the brightness observed at target 1 is from OH fluorescing outside the ring atmosphere, $n_0$ is reduced to 100 to 200 $cm^{-3}$, and generally, $n_0$ is restricted to the range 100 to 900 $cm^{-3}$. Integrating over the entire distribution gives a total number of OH molecules of roughly $\mathcal{N} = 0.7 \times 10^{33}$ to $6 \times 10^{33}$. For a steady-state distribution, OH must be produced at the same rate that it is lost, and the production rate is $P = \mathcal{N}/T$, where *T* is the mean lifetime of ring-atmosphere OH molecules. If physical adhesion to icy ring particles during collisions limits the lifetime, as has been argued for ring-atmosphere H atoms (*25*), then the Keplerian orbital period provides a reasonable lower limit to the OH lifetime, $T > 4 \times 10^4$ s. However, if the OH molecules are orbiting just outside of the main ring system, their lifetime is not limited by collisions with ring particles but by destructive interactions with magnetospheric charged particles (*6, 26*) and solar photons (*27*). Neglecting charged-particle destruction yields an upper limit of $T < 3 \times 10^7$ s (*27*). These lifetime limits restrict the production rate to $2 \times 10^{25} < P < 2 \times 10^{29}$ $s^{-1}$, or roughly $10^{25}$ to $10^{29}$ gaseous OH molecules per second. This large range reflects the uncertainties inherent in this preliminary analysis, but a more rigorous approach should yield a much more refined estimate. Model calculations (*8, 11, 12, 14, 26*) indicate that the OH distribution is a complicated function of the rates at which the rings and inner satellites produce gas, the distribution of energies imparted to newly produced molecules, and the OH molecule lifetime in the Saturn system.

### REFERENCES AND NOTES


1. C. B. Pilcher, C. R. Chapman, L. A. Lebofsky, H. H. Kieffer, *Science* **167**, 1372 (1970); R. N. Clark, *Icarus* **44**, 388 (1980).
2. M. Dennefeld, in *Exploration of the Planetary Systems*, A. Woszczyk and C. Iwaniszewski, Eds. (Int. Astron. Union Symp. 65, Reidel, Dordrecht, 1974), pp. 471–472; J. Blamont, in *The Rings of Saturn* (NASA SP-343, Washington, DC, 1974), pp. 125–130. For a discussion that preceded the definitive determination of the icy composition of the rings, see H. Harrison and R. I. Schoen, *Science* **157**, 1175 (1967).
3. H. Weiser, R. C. Vitz, H. W. Moos, *Science* **197**, 755 (1977); D. L. Judge, F.-M. Wu, R. W. Carlson, *ibid.* **207**, 431 (1980).
4. A. L. Broadfoot *et al.*, *ibid.* **212**, 206 (1981).
5. See A. F. Cheng, L. J. Lanzerotti, V. Pirronello, *J. Geophys. Res.* **87**, 4567 (1982), and references therein.
6. A. J. Lazarus and R. L. McNutt Jr., *ibid.* **88**, 8831 (1983); J. D. Richardson, A. Eviatar, G. L. Siscoe, *ibid.* **91**, 8749 (1986); R. E. Johnson *et al.*, *Icarus* **77**, 311 (1989); A. Eviatar and J. D. Richardson, *Ann. Geophys.* **8**, 725 (1990); G. E. Morfill, O. Havnes, C. K. Goertz, *J. Geophys. Res.* **98**, 11285 (1993); Z. Gan-Baruch, A. Eviatar, J. D. Richardson, R. L. McNutt Jr., *ibid.* **99**, 11063 (1994).
7. T. G. Northrop and J. R. Hill, *J. Geophys. Res.* **87**, 6045 (1982); W.-H. Ip, *ibid.* **88**, 819 (1983); J. E. P. Connerney and J. H. Waite, *Nature* **312**, 136 (1984); J. E. P. Connerney, *Geophys. Res. Lett.* **13**, 773 (1986).
8. D. E. Shemansky and D. T. Hall, *J. Geophys. Res.* **97**, 4143 (1992); D. A. Hilton and D. M. Hunten, *Icarus* **73**, 248 (1988); W. H. Smyth and M. L. Marconi, *ibid.* **101**, 18 (1993); W.-H. Ip, *Astrophys. J.* **457**, 922 (1996).
9. G. E. Morfill, H. Fechtig, E. Grün, C. K. Goertz, *Icarus* **55**, 439 (1983); P. K. Haff and A. Eviatar, *ibid.* **66**, 258 (1986).
10. T. G. Northrop and J. E. P. Connerney, *ibid.* **70**, 124 (1987).
11. M. K. Pospieszalska and R. E. Johnson, *ibid.* **93**, 45 (1991).
12. W.-H. Ip, *ibid.* **115**, 295 (1995); *J. Geophys. Res.* **89**, 8843 (1984).
13. J. N. Cuzzi and R. H. Durisen, *Icarus* **84**, 467 (1990); L. Dones, *ibid.* **92**, 194 (1991).
14. D. E. Shemansky, P. Matheson, D. T. Hall, H.-Y. Hu, T. M. Tripp, *Nature* **363**, 329 (1993).
15. For a detailed discussion of the OH $A^2\Sigma^+$-$X^2\Pi$ fluorescence process and emission rates, see D. G. Schleicher and M. F. A'Hearn, *Astrophys. J.* **331**, 1058 (1988).
16. R. E. Johnson, D. E. Grosjean, S. Jurac, R. A. Baragiola, *Eos* **74**, 569 (1993); M. Shi *et al.*, *J. Geophys. Res.* **100**, 26387 (1995).
17. D. P. Hamilton and J. A. Burns, *Nature* **365**, 498 (1993); also see *Science* **264**, 550 (1994).
18. D. E. Shemansky and P. L. Matheson, in *Calibrating Hubble Space Telescope: Post Servicing Mission*, A. Koratkar and C. Leitherer, Eds. (Space Telescope Science Institute, Baltimore, MD, 1995), pp. 88–93.
19. The HST WFPC-2 team acquired images using the F300W filter during the 22 May 1995 ring-plane crossing event (HST images U2OO0101T and U2OO0103T) and the 10 August event (image U2OO0304M). Details on the scattered-light content were described in a private communication with J. T. Clarke (e-mail: clarke@sunshine.sprl.umich.edu).
20. To model the scattered light, we used a solar spectrum acquired in March 1995 by the Solar Stellar Irradiance Comparison Experiment on the Upper Atmospheric Research Satellite (*28*). The solar spectrum in the 2990 to 3200 Å region was multiplied by a factor $A_\lambda$ that accounted for albedo variations in the spectrum of the source of the scattered light and for any chromatic alteration that occurred as the light was scattered within the telescope assembly. We used the polynomial form

$$A_\lambda = \sum_{k=0}^{K} a_k(\lambda - \lambda_0)^k \quad (1)$$

where $\lambda$ is the wavelength, the $a_k$ are polynomial coefficients, and $\lambda_0$ = 2990 Å. The solar spectrum was shifted in wavelength by $\Delta\lambda$ to account for shifts introduced by the gradient of scattered light across the aperture, Doppler shifts from the different velocities of Saturn and Earth at the time of the observations, and any relative FOS and SOLSTICE wavelength calibration errors. After convolving the scattered-light model with the FOS line-spread function for extended sources, $\Delta\lambda$ and $a_k$ were determined by a least-squares analysis to find the best fit to the observed FOS spectra in two wavelength bands (2990 to 3060 and 3110 to 3200 Å) that bracket the OH $A^2\Sigma^+$-$X^2\Pi$ (0,0) emission. This procedure was performed for each target, and each model scattered-light spectrum was subtracted from the corresponding FOS spectrum. The derived $A_\lambda$ curves have gradients from −9.5 to −7.5% per 100 Å in the 2990 to 3200 Å wavelength range. To estimate the magnitude of the error introduced by the scattered-light removal process, linear and quadratic forms for $A_\lambda$ were used, and the differences in the residual emissions for these two cases were used as an indicator of the uncertainty of the derived OH $A^2\Sigma^+$-$X^2\Pi$ (0,0) brightness (Table 1).
21. Fluorescent OH $A^2\Sigma^+$-$X^2\Pi$ (0,0) band spectral distributions were taken from D. G. Schleicher, thesis, University of Maryland, College Park (1983).
22. The rayleigh is a unit of surface brightness equivalent to one million photons per square centimeter per second per 4π steradians. The flux received at a detector from a uniform diffuse source with brightness $B$ in rayleighs is $F = 10^6\ B\Omega/4\pi$ (photons cm$^{-2}$ s$^{-1}$), where $\Omega$ is the aperture's solid angle in steradians.
23. See J. N. Cuzzi *et al.*, in *Planetary Rings*, R. Greenberg and A. Brahic, Eds. (Univ. of Arizona Press, Tucson, AZ, 1984), pp. 73–199, and references therein.
24. Aperture-averaged brightnesses for individual target spectra were calculated by integrating model brightnesses over the 3.66–arc sec by 1.29–arc sec FOS aperture. The position angle of the long dimension of the aperture measured eastward from Saturn's north pole direction was 76.4° for targets 1, 2, and 3 and 88.0° for targets 4 and 5.
25. R. W. Carlson, *Nature* **283**, 461 (1980).
26. J. D. Richardson, *J. Geophys. Res.* **97**, 13705 (1992).
27. S. A. Budzien, M. C. Festou, P. D. Feldman, *Icarus* **107**, 164 (1994).
28. G. J. Rottman, T. N. Woods, T. P. Sparn, *J. Geophys. Res.* **98**, 10667 (1993); T. N. Woods, G. J. Rottman, G. Ucker, *ibid.*, p. 10679.


29. We would like to thank A. Roman, A. Lubenow, and the Space Telescope Moving Object Support team at the Space Telescope Science Institute for making the 1995 Saturn ring-plane crossing observations possible and J. Clarke for providing information on the scattered-light content of WFPC-2 images. Support for this work was provided by NASA through grant GO-06015.01-94A from the Space Telescope Science Institute, which is operated by the Association of Universities for Research in Astronomy under NASA contract NAS5-26555.

19 December 1995; accepted 14 March 1996


# Observations of Saturn's Inner Satellites During the May 1995 Ring-Plane Crossing


Amanda S. Bosh and Andrew S. Rivkin



**The 22 May 1995 Saturn ring-plane crossing was observed with the Hubble Space Telescope; the markedly reduced scattered light from the rings at this time allowed study of the small inner satellites of the Saturn system. Prometheus was further from its predicted location than expected based on uncertainties in the 1981 ephemerides propagated forward by 15 years. A body found orbiting near or within Saturn's F ring is either an F-ring shepherd or a transient clump of dust within the F ring; given its approximate brightness, the clump theory is more likely.**


On 22 May 1995, the Earth passed through the plane of Saturn's rings, allowing us to view them in an edge-on configuration. During this time, the usually bright rings become faint, making this an ideal time to study the small inner satellites. These satellites have poorly defined ephemerides because they have rarely been observed. Discovered with ground-based telescopes during the 1966 and 1980 Saturn ring-plane crossings (*1, 2*) and by Voyagers 1 and 2 (*3*), these satellites include Pan, orbiting within the Encke gap; Atlas, just outside the outer edge of the A ring; Prometheus and Pandora, the F ring shepherds; Janus and Epimetheus, the coorbital satellites; Telesto and Calypso, at Tethys's $L_4$ and $L_5$ Lagrange points; and Helene, at Dione's $L_4$ point (*4*). Only Janus, Epimetheus, Telesto, Calypso, and Helene have been observed since 1980 (*5, 6*), leading to better determinations of libration parameters for these bodies.

For Atlas, Prometheus, Pandora, Janus, Epimetheus, Telesto, and Calypso, we examine the differences between observed and predicted locations in images of the Saturn system taken with the Wide Field–Planetary Camera 2 (WFPC2) (*7*) on the Hubble Space Telescope (HST). The Saturn system was observed on 22 May 1995 for 11 hours spanning the time of the Earth ring-plane crossing (*8*) and on 22 Novem-


A. S. Bosh, Lowell Observatory, Flagstaff, AZ 86001-4499, USA.

A. S. Rivkin, Lowell Observatory, Flagstaff, AZ 86001-4499, and Lunar and Planetary Laboratory, University of Arizona, Tucson, AZ 85721, USA.